

Magnetic-Moment Distribution in NiFe and AuFe Alloys*

J. W. Cable and E. O. Wollan†

Solid State Division, Oak Ridge National Laboratory, Oak Ridge, Tennessee 37830

(Received 13 October 1972)

We have determined the magnetic form factors and the corresponding magnetic-moment distributions for ordered Ni₃Fe and for disordered NiFe and AuFe alloys in an attempt to establish the variation of the individual atomic-moment distributions with composition. The results confirm the individual moments previously determined for NiFe alloys by neutron-diffuse-scattering methods and provide an upper limit of $0.03\mu_B$ for the Au moment in a 25-at. % Fe in Au alloy. A small negative moment density between atoms was found for all of the alloys studied. The symmetry of the moment distributions was determined at the Ni and Fe sites in ordered Ni₃Fe and for Fe in Au_{0.75}Fe_{0.25}. The Fe moment distribution is nearly spherical in both cases (54% T_{2g} in Ni₃Fe and 56% T_{2g} in the AuFe alloy) while the Ni moment distribution is strongly distorted. There seems to be little difference between the individual moment distributions in ordered and disordered Ni₃Fe. In both, the effective T_{2g} character decreases relative to pure Ni. The Ni d -function populations in ordered Ni₃Fe suggest that this decreasing T_{2g} character is associated with the larger size of, and the stronger d - d overlap with, the Fe atoms. The Ni $d(xz)$ and $d(yz)$ functions that are directed toward nearest-neighbor Ni atoms have essentially the same population as in pure Ni while the $d(xy)$ function directed toward nearest-neighbor Fe atoms loses population to $d(x^2 - y^2)$. Thus, there is a repulsion of spin-up electrons away from the regions of strong overlap.

I. INTRODUCTION

Accurate measurements of magnetic form factors and corresponding spin distributions constitute one of the important checks on the significance of various approaches to band-theory calculations for the ferromagnetic transition-group metals and alloys. Such measurements show spin distributions characterized by large positive densities localized at the atomic sites with small negative densities between atoms.¹⁻⁴ Observed asymmetries in the positive densities show an increasing T_{2g} character in proceeding across the series from bcc Fe (47% T_{2g})¹ to fcc Ni (81% T_{2g})³ and this behavior is successfully reproduced by band-structure calculations for the pure metals.^{5,6}

In this experiment we determine the spin-density distributions of some fcc NiFe and AuFe alloys. We attempt to establish the extent to which the individual atoms retain their spin distributions with varying composition. There is conflicting evidence on this point. Recent measurements⁴ on disordered CoNi alloys are most readily explained by assuming that both the average moment and average T_{2g} character are simply the weighted averages of the individual atomic properties as in a minimum-polarity rigid-band model. However, band-structure calculations for ferromagnetic disordered NiFe alloys suggest a rapidly decreasing T_{2g} symmetry of the Ni as Fe is added.⁷ Since only average moment densities are determined for disordered alloys, the above-mentioned interpretation for the CoNi system is not unique as far as

the symmetry is concerned. In this experiment we attempt to avoid this ambiguity by comparison with individually determined moment distributions for ordered Ni₃Fe and a 25-at. % Fe in Au alloy for which it is assumed that the Au atoms have no moments. The data are compared with previous diffuse-scattering measurements and the band-structure results.

II. EXPERIMENTAL

A. Sample Preparation

Single crystals of NiFe alloys containing 25- and 50-at. % Fe and of a AuFe alloy with 25-at. % Fe were grown by the strain-anneal method. After annealing and quenching to room temperature, portions of the samples were subjected to chemical, x-ray, and electron-probe analyses which showed them to be single-phase fcc, homogeneous in the micron range, and within 0.5 at. % of the nominal concentrations. Pillar-shaped diffraction specimens with typical dimensions of about $0.5 \times 0.5 \times 6$ mm were cut from some of the larger grains. The AuFe specimen was cut with a [110] direction parallel to the pillar axis while the NiFe crystals were unoriented. These crystals showed mosaic spreads of about 0.4° .

In addition, a single-crystal ingot of a NiFe alloy containing 25-at. % Fe and 75-at. % ⁶⁰Ni was grown from the melt. This isotopic crystal was necessary for the measurements on the ordered alloy for which the nuclear Bragg scattering consists of fundamental reflections with intensities

proportional to $(b_{\text{Fe}} + 3b_{\text{Ni}})^2$ and superlattice reflections with intensities proportional to $(b_{\text{Fe}} - b_{\text{Ni}})^2 S^2$, where the b 's are the nuclear-scattering amplitudes, and S is the long-range-order parameter. Because of the nearly equal nuclear amplitudes of Fe (0.951×10^{-12} cm) and Ni (1.03×10^{-12} cm), the superlattice reflections are only about 10^{-4} as intense as the fundamentals. We have therefore used $^{60}\text{Ni}_3\text{Fe}$ ($b_{\text{Ni}} = 0.282 \times 10^{-12}$ cm) for enhancement of the superlattice intensities.

The development of long-range order in Ni_3Fe is notoriously sluggish and complete order does not seem attainable by the usual heat-treatment methods. Fortunately, the saturation magnetizations of the ordered and disordered alloys differ by only 5%,³ so we can reasonably expect only small changes in the Fe and Ni moments with local environment and an adequate representation of the individual moment distributions from measurements on the partially ordered alloy. The ordering kinetics of Ni_3Fe have been reported by Gomankov, Puzey, and Loshmanov⁹ who used neutron-diffraction methods and isotopic samples to determine long-range-order parameters. They report a first-order phase transition at 490°C and ordering in two stages: (i) the growth of antiphase domains and (ii) the establishment of order inside the domains. The highest degree of order and the largest domain size is attained by annealing near 490°C . For a 100-h anneal at 470°C they report $S = 0.70$ and antiphase domain boundaries separated by more than 200 \AA . Similarly, Treuting and Batterman¹⁰ report $S = 0.73$ and 60-\AA antiphase domains for a sample annealed for 1 week at 490°C . Our results generally agree with these previous observations. Crystals annealed for 200 h at 450°C , 500 h at 425°C , and 700 h at 400°C showed broad superlattice lines [5° in the (100) rocking curve] corresponding to 25-\AA antiphase domains and $S = 0.60$. One crystal was annealed for 24 h at 1200°C and 100 h at 475°C . The mosaic spread decreased from 0.4° to 0.15° and the antiphase domain size increased to about 60 \AA . We were unable to obtain domains larger than 60 \AA and expect that the larger domain sizes previously inferred⁹ result from the disc-shaped diffraction spots in reciprocal space and the polycrystalline techniques used in those measurements.

B. Magnetic-Structure-Factor Measurements

The magnetic-structure-factor measurements were made by the standard polarized-neutron technique¹¹ in which the sample is magnetized vertically, and the ratio of the Bragg-reflection intensities for incident spin-up and spin-down neutrons is determined in the horizontal scattering plane. This so-called flipping ratio is given by $R = (p + b)^2 /$

$(p - b)^2$ and the magnetic-scattering amplitudes p are obtained from R by use of the known nuclear-scattering amplitudes b . The measurements were made at the polarized-beam spectrometer at the high-flux isotope reactor using a magnetizing field of 8 kOe and neutron wavelengths of 0.768, 0.978, and 1.067 \AA . All measurements were made at room temperature except those for the 25-at.% Fe in Au alloy for which $T_c \approx 300^\circ\text{K}$.¹² These were made at 100°K . The observed flipping ratios were corrected for incomplete incident polarization ($\sim 0.5\%$) and spin reversal ($\sim 0.5\%$) and for depolarization in the sample. The latter was also $\sim 0.5\%$ for all of the samples except for $\text{Ni}_{0.5}\text{Fe}_{0.5}$ which was mounted with the pillar axis 26° from the field direction and for which the sample depolarization was about 2%. Checks for possible extinction effects were made by missetting the Bragg angle, by varying the path length through crystals of different thickness, and by changing the neutron wavelength. These showed that extinction was negligible for all crystals with large mosaic spread ($\sim 0.4^\circ$). The $^{60}\text{Ni}_3\text{Fe}$ crystal with 0.15° mosaic spread showed some extinction for the fundamentals.

III. RESULTS

A. Ordered $^{60}\text{Ni}_3\text{Fe}$

Measurements were made for the first 21 fundamental reflections out to $\sin\theta/\lambda \approx 1.00$ and for the first 24 superlattice reflections to about $\sin\theta/\lambda = 0.81$. In obtaining some of these reflections, it was necessary to tilt the magnet away from the vertical direction and for these an additional q^2 correction was applied. The data are summarized in Table I which represents a weighted average of the data from three crystals. The data are presented in the form of both p/b , the magnetic to-nuclear-scattering-amplitude ratio, and F , the magnetic structure factor in Bohr magnetons per unit cell. The F values are given by $(0.2695)^{-1} \times (b_{\text{Fe}} + 3b_{\text{Ni}})p/b$ for the fundamentals and by $(0.2695)^{-1} \times (b_{\text{Fe}} - b_{\text{Ni}})p/b$ for the superlattice reflections. Quoted errors include both counting statistics and estimated error limits in the various corrections.

Both the fundamental and superlattice reflections exhibit structure-factor variations for pairs of reflections at the same $\sin\theta/\lambda$ values indicating asphericities in both the sum and difference moment densities. This is much more pronounced for the superlattice lines as would be expected if the previously reported asymmetries of the pure metals are retained in the alloy. The asymmetries are illustrated in Fig. 1 which shows the magnetic-moment density along certain crystallographic directions as obtained by Fourier transforming

the data of Table I. The moment density measured from an Fe site shows an expansion along the $\langle 100 \rangle$ directions relative to $\langle 110 \rangle$. This corresponds to an atom in a cubic site with excess E_g character. The Ni atom shows an interesting tetragonal distortion in moment density with a contraction along $[001]$ relative to both $[100]$ and $[110]$. We should note that the local symmetry at

TABLE I. Summary of magnetic-structure-factor measurements for $^{60}\text{Ni}_3\text{Fe}$ (ordered).

hkl	$\frac{\sin\theta}{\lambda}$	$\frac{b}{a}$	$F_{\text{obs.}} \left(\frac{\mu_B}{\text{unit cell}} \right)$	$F_{\text{calc.}}^a$
111	0.244	0.480	3.20 ± 0.03	3.23
200	0.281	0.424	2.82 ± 0.02	2.79
220	0.398	0.243	1.620 ± 0.013	1.65
311	0.467	0.177	1.177 ± 0.010	1.14
222	0.487	0.158	1.053 ± 0.007	1.04
400	0.563	0.103	0.683 ± 0.007	0.645
331	0.613	0.072	0.476 ± 0.007	0.501
420	0.629	0.065	0.430 ± 0.007	0.436
422	0.689	0.044	0.290 ± 0.007	0.291
511	0.731	0.027	0.177 ± 0.007	0.186
333	0.731	0.030	0.200 ± 0.007	0.214
440	0.796	0.014	0.093 ± 0.007	0.104
531	0.832	0.007	0.047 ± 0.013	0.061
600	0.844	0.004	0.027 ± 0.013	0.029
442	0.844	0.010	0.067 ± 0.013	0.061
620	0.890	-0.005	-0.033 ± 0.020	0.004
533	0.923	-0.002	-0.013 ± 0.013	0.002
622	0.933	-0.004	-0.027 ± 0.007	-0.018
444	0.975	-0.005	-0.033 ± 0.013	-0.011
551	1.005	-0.008	-0.053 ± 0.013	-0.028
711	1.005	-0.011	-0.073 ± 0.013	-0.054
100	0.141	0.778	1.93 ± 0.04	1.96
110	0.191	0.660	1.64 ± 0.03	1.63
210	0.315	0.399	0.990 ± 0.012	0.981
211	0.345	0.337	0.836 ± 0.012	0.813
221	0.422	0.196	0.487 ± 0.005	0.491
300	0.422	0.217	0.539 ± 0.005	0.537
310	0.445	0.190	0.472 ± 0.005	0.474
320	0.507	0.123	0.305 ± 0.005	0.293
321	0.526	0.108	0.268 ± 0.005	0.257
322	0.580	0.065	0.161 ± 0.005	0.150
410	0.580	0.097	0.241 ± 0.005	0.236
330	0.597	0.036	0.089 ± 0.005	0.099
411	0.597	0.062	0.154 ± 0.005	0.159
421	0.645	0.029	0.072 ± 0.005	0.089
332	0.660	0.013	0.032 ± 0.005	0.035
430	0.703	0.031	0.077 ± 0.005	0.062
500	0.703	0.020	0.050 ± 0.005	0.073
431	0.717	0.012	0.030 ± 0.005	0.030
510	0.717	0.038	0.094 ± 0.005	0.098
432	0.758	0.000	0.000 ± 0.005	-0.010
520	0.758	0.006	0.015 ± 0.005	0.021
521	0.771	0.019	0.047 ± 0.005	0.040
441	0.808	-0.033	-0.082 ± 0.005	-0.068
522	0.808	-0.007	-0.017 ± 0.005	-0.016

^aSee text for relevant parameters.

the Ni sites is D_{4h} with mutually perpendicular tetragonal axes for the three sites. The directions given in Fig. 1 are defined so that $[001]$ is parallel to the tetragonal axis at each Ni site.

A more complete description of the moment distribution is shown by the magnetic-moment density maps in Fig. 2. Contours are in $\mu_B/\text{\AA}^3$ with the positive contours representing point densities and the zero contours corresponding to an average over a sphere of radius 0.44\AA . The moment density around the Fe atom at 000 and the Ni atom at $0\frac{1}{2}\frac{1}{2}$, for which the tetragonal axis is perpendicular to the plane of the figure, is shown in Fig. 2(b). In this plane, there is little indication of a departure from spherical symmetry around the Ni atoms. However, the Ni atoms at $\frac{1}{2}\frac{1}{2}0$ and $\frac{1}{2}0\frac{1}{2}$ in Fig. 2(a) show an appreciable contraction of moment density along the tetragonal axis of each site. These axes are indicated in the figure by the arrows labeled C_4 .

Local moments were determined by the method described by Moon¹³ in which the moment density above the background level between atoms is integrated around the atomic sites. The Fourier sums were made as a function of the number of structure-factor terms included in the sum and of the radius of the averaging sphere. The background was taken at $\frac{1}{2}00$. Convergence was noted for more than about 30 terms and moment values were therefore taken as the average of the last 14 terms in the series. For averaging sphere radii between 0.35 and 0.70\AA the local moment per unit cell remains constant at $(5.12 \pm 0.04) \mu_B$ and the average moment density at $\frac{1}{2}00$ approaches $-0.0062 \mu_B/\text{\AA}^3$. The average moments within spheres centered at 000 (Fe site) and $\frac{1}{2}\frac{1}{2}0$ (Ni site) were determined as a function of sphere radii out to the midpoint between atoms. The Ni moment reached a constant value of $(0.679 \pm 0.005) \mu_B$ for radii greater than 1\AA , while the Fe moment reached only $2.7 \mu_B$ and was still increasing at the midpoint (1.256\AA). We conclude that this summation gives an adequate description of the local Ni moment but does not include all of the local Fe moment because of the larger size of the Fe atom. Except for a small correction for the nonuniformity of the nonlocal-moment density, i. e., the overlapping tails of positive-moment density in the $\langle 110 \rangle$ directions and some structure near $\frac{1}{2}\frac{1}{2}\frac{1}{2}$, the Fe moment is simply the difference between the local moment per unit cell and the Ni moments. Thus $\mu_{\text{Fe}} \sim 5.12 - 3(0.679) = 3.08 \mu_B/\text{Fe atom}$.

The magnetic form factors of the ferromagnetic transition metals are described remarkably well by a model in which free-atom spin densities with appropriately populated crystal field sublevels are superimposed on a uniform negative spin den-

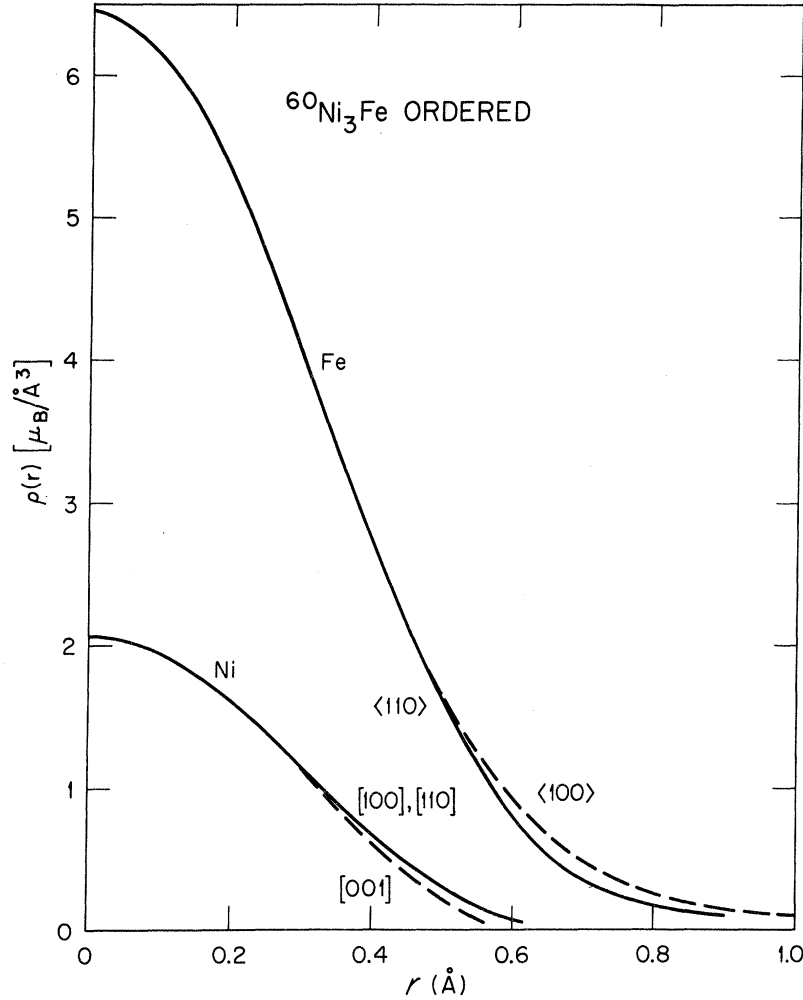


FIG. 1. Magnetic-moment density as a function of distance along some major symmetry directions in ordered Ni_3Fe . The different brackets around the indices indicate an equivalence of crystallographic directions at the Fe site that is absent at the Ni sites.

sity.¹⁻³ Although the success of this model is not understood and some ambiguity remains in the s - or d -like character of both the positive and negative density regions,⁶ it nevertheless provides the best representation of the observed moment densities of any current model. We now proceed to this type of analysis for Ni_3Fe . In the Ni_3Fe structure the Fe atoms preferentially occupy the β sites at 000 while the Ni atoms prefer the α sites at $\frac{1}{2}\frac{1}{2}0$, $\frac{1}{2}0\frac{1}{2}$, and $0\frac{1}{2}\frac{1}{2}$. In the perfectly ordered state, the octahedral crystal field at the β sites splits the d orbitals into $T_{2g}[d(xy), d(xz), d(yz)]$ and $E_g[d(x^2-y^2), d(z^2)]$ symmetry types, while the tetragonal field at the α sites gives a splitting into $A_{1g}[d(z^2)]$, $B_{1g}[d(x^2-y^2)]$, $B_{2g}[d(xy)]$, and $E_g[d(xz), d(yz)]$ symmetry types. The magnetic structure factors (in Bohr magnetons) for the fundamental (F_{NL}) and superlattice (F_{SL}) reflections can be derived from the principal scattering factors given by Weiss and Freeman¹⁴ and assume the form

$$F_{\text{NL}} = \mu_{\text{Fe}} \langle j_0 \rangle_{\text{Fe}} + \mu_{\beta} \left(\frac{5}{2} \gamma_{\beta} - 1 \right) A_{hkl} \langle j_4 \rangle_{\beta} + 3 \mu_{\text{Ni}} \langle j_0 \rangle_{\text{Ni}} + \mu_{\alpha} \delta_{\alpha} B_{hkl} \langle j_4 \rangle_{\alpha},$$

$$F_{\text{SL}} = \mu_{\text{Fe}} \langle j_0 \rangle_{\text{Fe}} + \mu_{\beta} \left(\frac{5}{2} \gamma_{\beta} - 1 \right) A_{hkl} \langle j_4 \rangle_{\beta} - \mu_{\text{Ni}} \langle j_0 \rangle_{\text{Ni}} + \mu_{\alpha} \epsilon_{\alpha} C_{hkl} \langle j_2 \rangle_{\alpha} + \mu_{\alpha} \delta_{\alpha} D_{hkl} \langle j_4 \rangle_{\alpha}.$$

Here, the $\langle j_n \rangle$ are the radial integrals tabulated for the free atoms by Freeman and Watson¹⁵ and the μ 's are the magnetic moments at the α and β sites. The symmetry parameters are

$$\gamma = E_g$$

for cubic sites and

$$\delta = A_{1g} + \frac{1}{6} B_{1g} + \frac{1}{6} B_{2g} - \frac{2}{3} E_g,$$

$$\epsilon = A_{1g} - B_{1g} - B_{2g} + \frac{1}{2} E_g$$

for tetragonal sites, where the fractional populations of the symmetry functions are represented by the respective point-group symbols. The geometrical factors are

$$A_{hkl} = \frac{h^4 + k^4 + l^4 - 3(h^2k^2 + h^2l^2 + k^2l^2)}{h^2 + k^2 + l^2},$$

$$B_{hkl} = \frac{3}{4} (5G - 3),$$

$$C_{hkl} = \frac{10}{7} (3 \cos^2 \phi - 1),$$

$$D_{hkl} = \frac{9}{28} (35G - 70 \cos^4 \phi + 60 \cos^2 \phi - 27),$$

with

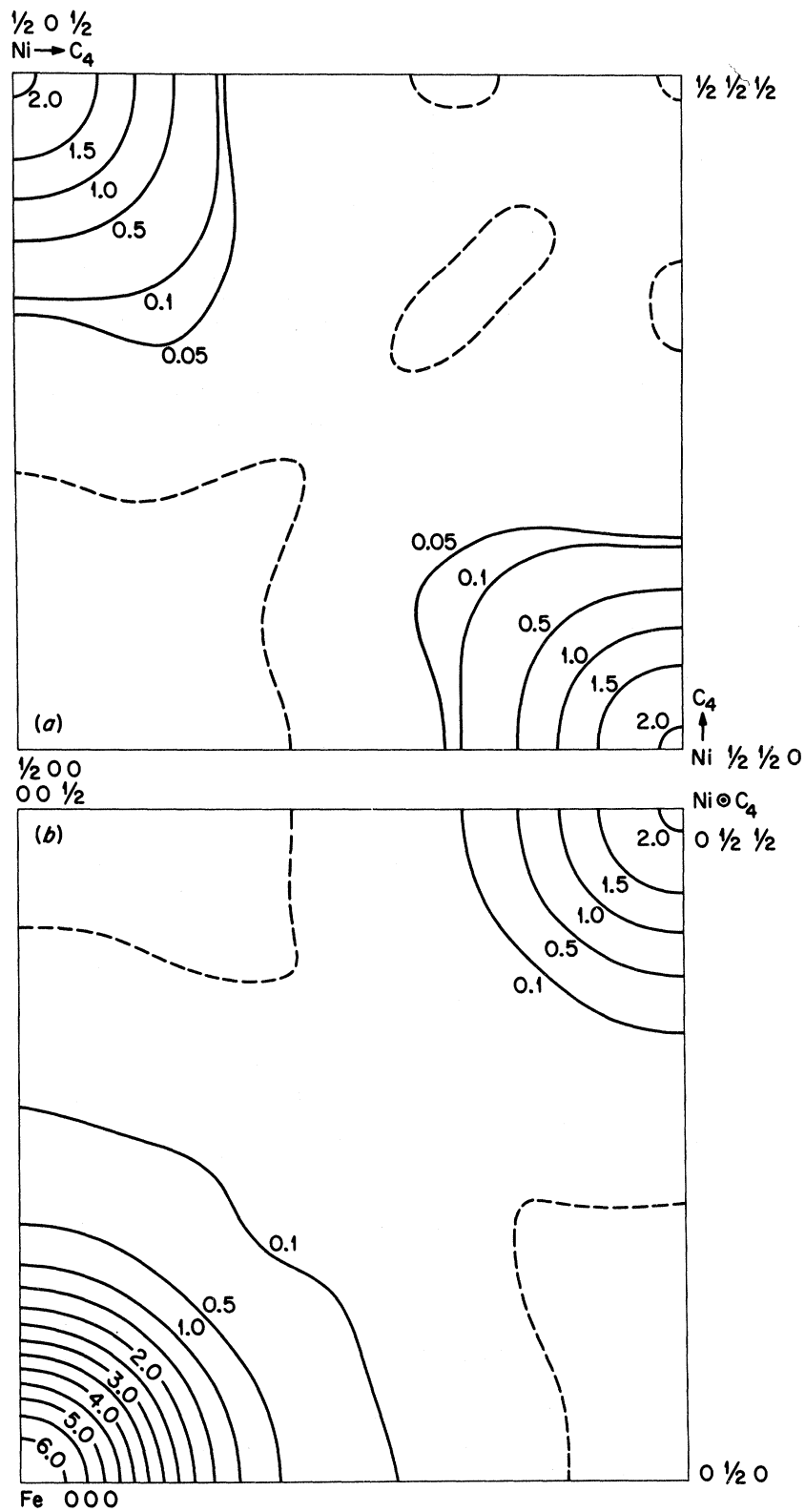


FIG. 2. Magnetic-moment-density maps in parallel (100) planes of ordered Ni₃Fe. Contour lines are labeled in units of $\mu_B/\text{\AA}^3$. Positive contours (solid lines) represent point densities while the zero contours (dashed lines) represent an average density within a sphere of radius 0.44 Å. The arrows labeled C_4 at the Ni-atom positions indicate the direction of the tetragonal axis at that site.

$$G = \frac{h^4 + k^4 + l^4}{(h^2 + k^2 + l^2)^2}$$

and

$$\cos^2 \phi = \frac{h^2}{h^2 + k^2 + l^2}$$

Here, we use the convention that h is odd for the odd-even-even and even for the even-odd-odd superlattice reflections. We have least-squares fitted the observed structure factors to these expressions substituting for $\langle j_0 \rangle$ the experimental Fe and Ni spherical form factors (including orbital contributions) as tabulated by Moon.¹³ The Hartree-Fock $\langle j_2 \rangle$ and $\langle j_4 \rangle$ functions¹⁵ were used for Fe⁺² at the β sites and Ni⁺² at the α sites. Fi-

nally, $\mu_\beta = (2/g_{\text{Fe}})\mu_{\text{Fe}}$, $\mu_\alpha = (2/g_{\text{Ni}})\mu_{\text{Ni}}$ for the fundamentals and $S\mu_\beta = (2/g_{\text{Fe}})\mu_{\text{Fe}}$, $S\mu_\alpha = (2/g_{\text{Ni}})\mu_{\text{Ni}}$ for the superlattice reflections. We have taken the g values of the pure metals, $g_{\text{Fe}} = 2.075$ and $g_{\text{Ni}} = 2.18$. The following parameters were obtained:

$$\mu_{\text{Fe}} = 3.10 \pm 0.01, \quad \mu_{\text{Ni}} = 0.682 \pm 0.005,$$

$$\frac{5}{2}\gamma_\beta - 1 = 0.102 \pm 0.019,$$

$$\delta_\alpha = -0.196 \pm 0.026, \quad \epsilon_\alpha = 0.008 \pm 0.018.$$

The structure factors calculated with these parameters are compared with the observed values in Fig. 3 and Table I.

The partially ordered state is actually more complicated than this model because of the occur-

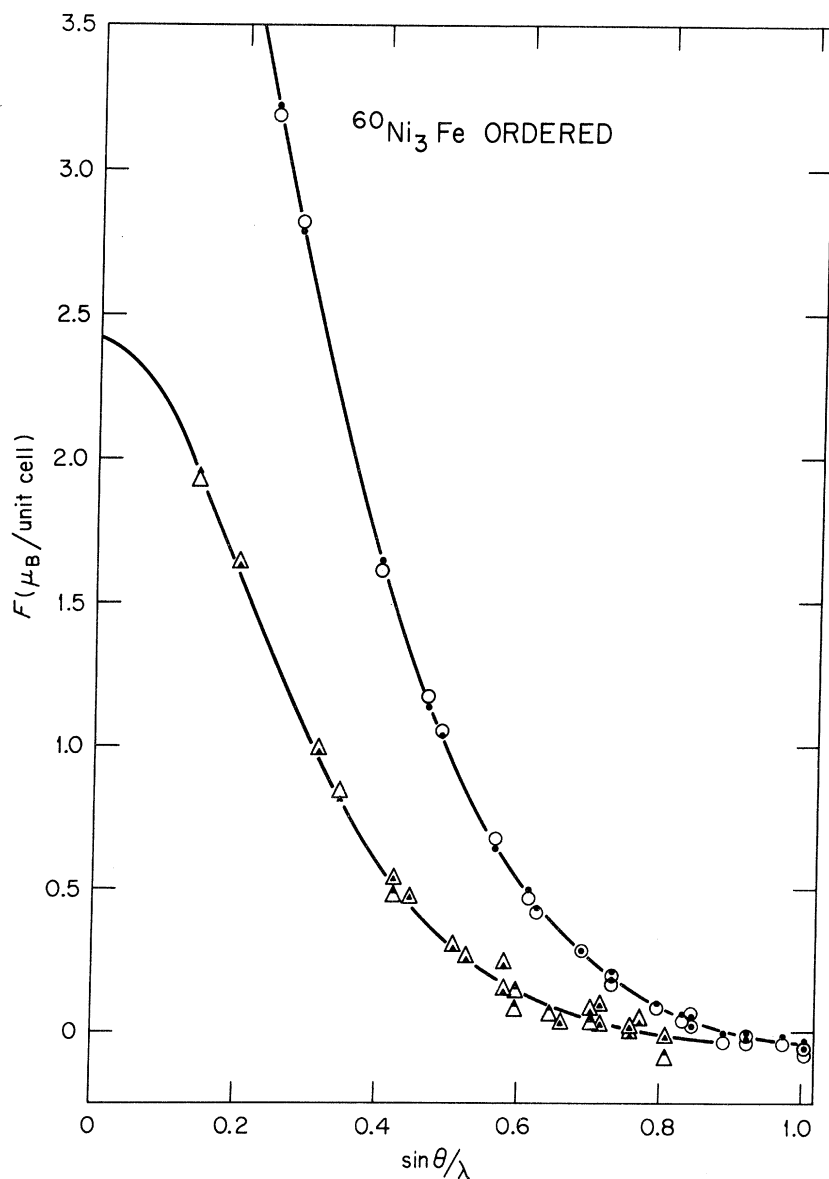


FIG. 3. Comparison of the observed (open points) and calculated (closed points) magnetic-structure factors of ordered Ni_3Fe . The curves show the expected scattering for spherical-moment distributions while the departures from these curves represent the aspherical components. The circles refer to the fundamentals and the triangles to the superlattice reflections.

rence of local symmetries other than octahedral or tetragonal. However, if we assume that the local symmetries of the α and β sites remain unchanged for the partially ordered state, then the apparent asymmetry parameters become

$$\frac{5}{2}\gamma_{\beta} - 1 \simeq r_{\beta} \left(\frac{5}{2}\gamma_{\text{Fe}} - 1 \right) + w_{\beta} \frac{g_{\text{Fe}}}{g_{\text{Ni}}} \frac{\mu_{\text{Ni}}}{\mu_{\text{Fe}}} \left(\frac{5}{2}\gamma_{\text{Ni}} - 1 \right),$$

$$\delta_{\alpha} \simeq r_{\alpha} \delta_{\text{Ni}} + w_{\alpha} \frac{g_{\text{Ni}}}{g_{\text{Fe}}} \frac{\mu_{\text{Fe}}}{\mu_{\text{Ni}}} \delta_{\text{Fe}},$$

$$\epsilon_{\alpha} \simeq r_{\alpha} \epsilon_{\text{Ni}} + w_{\alpha} \frac{g_{\text{Ni}}}{g_{\text{Fe}}} \frac{\mu_{\text{Fe}}}{\mu_{\text{Ni}}} \epsilon_{\text{Fe}}.$$

Here $r_{\alpha} = \frac{1}{4}(S+3)$, $r_{\beta} = \frac{1}{4}(3S+1)$, $w_{\alpha} = 1 - r_{\alpha}$, $w_{\beta} = 1 - r_{\beta}$, and we let $\langle j_2 \rangle_{\text{Fe}} = \langle j_2 \rangle_{\text{Ni}}$ and $\langle j_4 \rangle_{\text{Fe}} = \langle j_4 \rangle_{\text{Ni}}$. With $S = 0.7$ and the fitted values of μ_{Fe} and μ_{Ni} it can be seen that misplaced Ni atoms on β sites have a negligible effect on the determination of γ_{Fe} while misplaced Fe atoms on α sites can significantly alter δ_{Ni} and ϵ_{Ni} . Independent evaluation of δ_{Ni} and δ_{Fe} or of ϵ_{Ni} and ϵ_{Fe} are not feasible but reasonable δ_{Ni} and ϵ_{Ni} values can be obtained by assuming that the d -orbital populations are the same for Fe atoms on α and β sites. The observed γ_{Fe} parameter (0.462 ± 0.013) corresponds to $\delta_{\text{Fe}} = 0.058$ and $\epsilon_{\text{Fe}} = 0.000$ and the Ni parameters are then $\delta_{\text{Ni}} = -0.234 \pm 0.028$ and $\epsilon_{\text{Ni}} = 0.009 \pm 0.020$. These define the orbital populations for the Ni atoms in tetragonal sites which are given by

$$A_{1g} = \frac{1}{7}(1.4 + 3.6\delta_{\text{Ni}} + 2\epsilon_{\text{Ni}}) = 0.08 \pm 0.02,$$

$$B_{1g} + B_{2g} = \frac{1}{7}(2.8 + 1.2\delta_{\text{Ni}} - 4\epsilon_{\text{Ni}}) = 0.36 \pm 0.02,$$

$$E_g = \frac{1}{7}(2.8 - 4.8\delta_{\text{Ni}} - 2\epsilon_{\text{Ni}}) = 0.56 \pm 0.02.$$

The B_{1g} and B_{2g} populations are not independently determined. However, the density maps show no anisotropy around the α sites in the xy plane [Fig. 2(b)], so equal populations may be reasonably assumed. For the Ni atoms then, the $(B_{2g} + E_g)$ functions, which correspond to the T_{2g} functions in octahedral symmetry, contain 74% of the unpaired electrons.

B. Disordered NiFe Alloys

Data were collected for the first 11 reflections with scattering vectors in the horizontal plane. The results are presented in Tables II and III in terms of both p/b values and structure factors in μ_B per atom. The limited amount of data for these samples is insufficient for obtaining density maps but enough to obtain the relevant parameters by analysis with assumed form factors. The individual asymmetry parameters γ_{Fe} and γ_{Ni} cannot be determined from these average scattering density data since $\langle j_4 \rangle_{\text{Fe}} \simeq \langle j_4 \rangle_{\text{Ni}}$ for all reflections. We therefore write the structure factors with an average aspherical term,

$$F_{hkl} = c_{\text{Fe}} \mu_{\text{Fe}} \langle j_0 \rangle_{\text{Fe}} + c_{\text{Ni}} \mu_{\text{Ni}} \langle j_0 \rangle_{\text{Ni}}$$

$$+ (2/\bar{g}) \bar{\mu} (\frac{5}{2}\bar{\gamma} - 1) A_{hkl} \langle \bar{j}_4 \rangle,$$

and least-squares fit the observations to this expression with the same form-factor assumptions as in Sec. III A. The parameters obtained are given below each table and the quality of the fit is indicated by comparison of the observed and calculated structure factors in Tables II and III and Figs. 4 and 5.

C. Disordered $\text{Au}_{0.75}\text{Fe}_{0.25}$

Data were collected for the first 16 reflections with scattering vectors perpendicular to $[110]$ and the results are summarized in Table IV and Fig. 6. Here, the magnetic structure factors are obtained from the p/b values by use of $b_{\text{Fe}} = 0.951 \times 10^{-12}$ cm and $b_{\text{Au}} = 0.76 \times 10^{-12}$ cm. These are well represented by the spin-polarized Hartree-Fock form factor¹⁸ of Fe^{+2} or, equivalently, the spin-only experimental form factor of bcc Fe¹³ and an average moment of $0.71 \mu_B/\text{atom}$. This exceeds the magnetization by $0.04 \mu_B/\text{atom}$ and suggests a negative polarization between atoms and a localization of the positive moments at the Fe sites with $2.84 \mu_B/\text{Fe}$ atom. If we assume the experimental Pt form factor¹⁷ for a possible $5d$ -like moment distribution on the Au atoms then the maximum moment consistent with these data is $0.03 \mu_B/\text{Au}$ atom. The differences between the magnetic structure factors for the paired reflections (511), (333) and (600), (442) give the asymmetry parameter $\gamma_{\text{Fe}} = 0.437 \pm 0.013$.

IV. DISCUSSION

In Secs. I-III we have seen that the magnetic structure factors of these NiFe and AuFe alloys are reproduced by assigning $3d$ -like spin densities with appropriately populated crystal field sublevels

TABLE II. Summary of magnetic-scattering-amplitude measurements for $\text{Ni}_{0.75}\text{Fe}_{0.25}$.

hkl	$\frac{\sin\theta}{\lambda}$	$\frac{p}{b}$	$F_{\text{obs.}} \left(\frac{\mu_B}{\text{atom}} \right)$	$F_{\text{calc.}}^a$
111	0.244	0.2084	0.781	0.783
200	0.281	0.1812	0.679	0.676
220	0.398	0.1045	0.392	0.398
311	0.466	0.0767	0.287	0.280
222	0.487	0.0682	0.256	0.250
400	0.562	0.0429	0.161	0.155
331	0.613	0.0287	0.108	0.120
422	0.689	0.0178	0.067	0.070
511	0.731	0.0109	0.041	0.042
333	0.731	0.0134	0.050	0.051
440	0.795	0.0063	0.024	0.026
			± 0.005	

$$^a F_{\text{calc.}} = c_{\text{Fe}} \mu_{\text{Fe}} f_{\text{Fe}} + c_{\text{Ni}} \mu_{\text{Ni}} f_{\text{Ni}} + (2/\bar{g}) \bar{\mu} (\frac{5}{2}\bar{\gamma} - 1) A_{hkl} \langle j_4 \rangle,$$

$$\mu_{\text{Fe}} = 3.13 \pm 0.15, \mu_{\text{Ni}} = 0.63 \pm 0.05, \bar{\gamma} = 0.375 \pm 0.017.$$

TABLE III. Summary of magnetic-scattering-amplitude measurements for $\text{Ni}_{0.5}\text{Fe}_{0.5}$.

hkl	$\frac{\sin\theta}{\lambda}$	$\frac{b}{b}$	$F_{\text{obs.}} \left(\frac{\mu_B}{\text{atom}} \right)$	$F_{\text{calc.}}^a$
111	0.242	0.2735	1.005	1.020
200	0.279	0.2453	0.902	0.886
220	0.395	0.1354	0.498	0.505
311	0.463	0.0990	0.364	0.356
222	0.483	0.0868	0.319	0.304
400	0.558	0.0574	0.211	0.219
331	0.608	0.0362	0.133	0.140
422	0.684	0.0225	0.083	0.079
511	0.725	0.0170	0.062	0.070
333	0.725	0.0098	0.036	0.044
440	0.789	0.0050	0.018	0.022
				± 0.005

$$^a F_{\text{calc.}} = c_{\text{Fe}} \mu_{\text{Fe}} f_{\text{Fe}} + c_{\text{Ni}} \mu_{\text{Ni}} f_{\text{Ni}} + (2/\sqrt{g}) \bar{\mu} (\frac{5}{2}\bar{\gamma} - 1) A_{hkl} \langle j_4 \rangle,$$

$$\mu_{\text{Fe}} = 2.54 \pm 0.16, \mu_{\text{Ni}} = 0.78 \pm 0.04, \bar{\gamma} = 0.456 \pm 0.012.$$

to the atomic sites. In addition, direct Fourier inversion of the ordered Ni_3Fe data yields the same moment values at the Fe and Ni sites and in the interatom region as those obtained from the form-factor analysis. In Table V we compare the moment values obtained from these data with previous magnetization^{8,12,18,19} and diffuse-neutron-

TABLE IV. Summary of magnetic-scattering-amplitude measurements for $\text{Au}_{0.75}\text{Fe}_{0.25}$.

hkl	$\frac{\sin\theta}{\lambda}$	$\frac{b}{b}$	$F_{\text{obs.}} \left(\frac{\mu_B}{\text{atom}} \right)$	$F_{\text{calc.}}^a$
111	0.216	0.1577	0.473	0.462
200	0.249	0.1345	0.403	0.407
220	0.352	0.0809	0.243	0.247
311	0.413	0.0594	0.178	0.176
222	0.431	0.0513	0.154	0.156
400	0.498	0.0368	0.110	0.108
331	0.543	0.0237	0.071	0.077
422	0.610	0.0147	0.045	0.046
511	0.647	0.0126	0.039	0.039
333	0.647	0.0095	0.029	0.031
440	0.704	0.0047	0.014	0.017
600	0.747	0.0065	0.019	0.016
442	0.747	0.0042	0.013	0.007
533	0.816	-0.0038	-0.011	-0.004
622	0.826	-0.0015	-0.005	0.000
444	0.863	-0.0020	-0.006	-0.008
				± 0.005

$$^a F_{\text{calc.}} = c_{\text{Fe}} \mu_{\text{Fe}} [\langle j_0 \rangle_{\text{Fe}} + (\frac{5}{2} \gamma_{\text{Fe}} - 1) A_{hkl} \langle j_4 \rangle_{\text{Fe}}], \mu_{\text{Fe}} = 2.84$$

$$\pm 0.04, \gamma_{\text{Fe}} = 0.437 \pm 0.013.$$

scattering²⁰ results. The individual Fe and Ni moments and the corresponding average moments are given in the first three data columns. In all cases

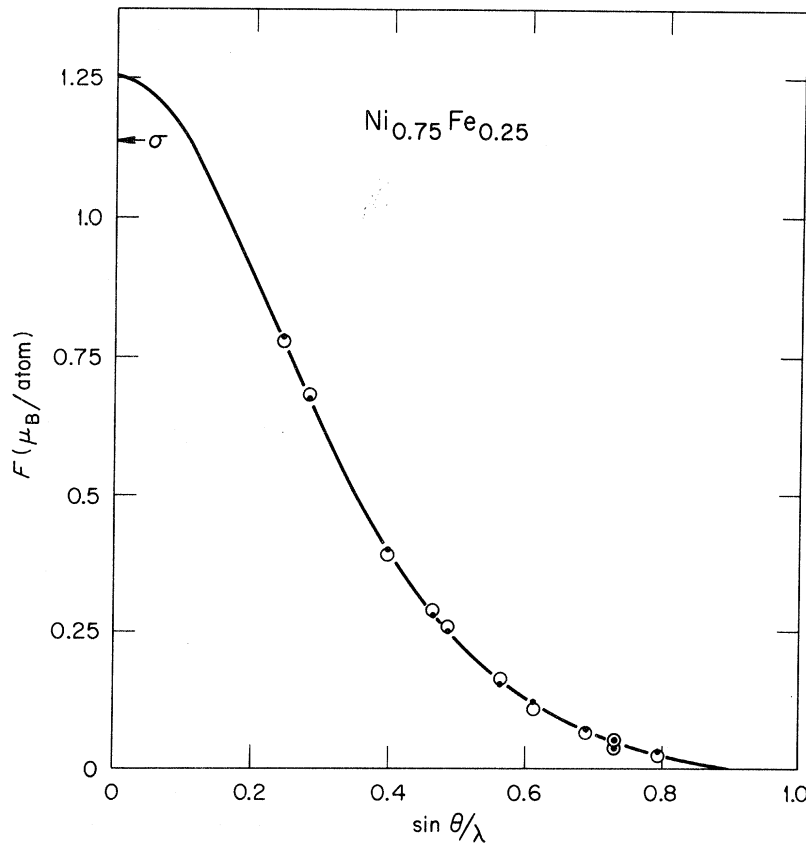


FIG. 4. Comparison of the observed (open points) and calculated (closed points) magnetic structure factors of disordered $\text{Ni}_{0.75}\text{Fe}_{0.25}$. The data show little departure from the spherical curve. The $\sin\theta/\lambda = 0$ value of the average moment is $0.10 \mu_B$ larger than the magnetization (Ref. 8) indicated by σ .

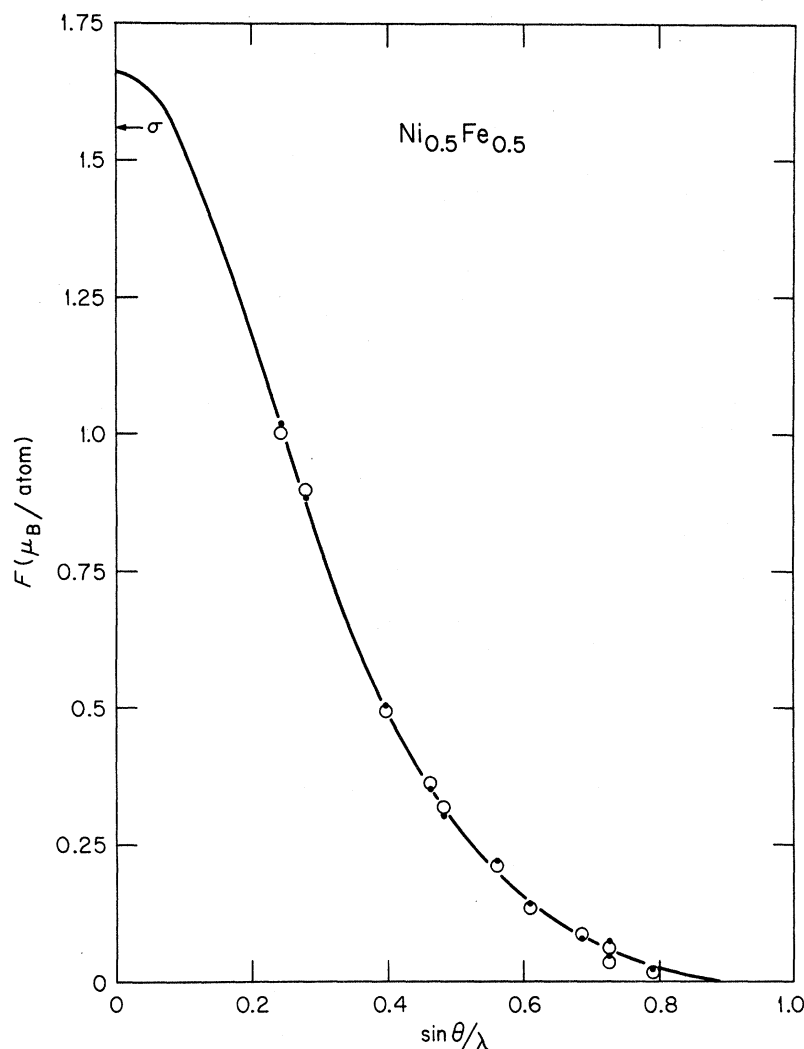


FIG. 5. Comparison of the observed (open points) and calculated (closed points) magnetic structure factors of disordered $\text{Ni}_{0.5}\text{Fe}_{0.5}$.

this average $3d$ -like moment is 6–8% larger than the average moment obtained from magnetization measurements (column 4). The difference corresponds to the non-local-moment density which is negative for each alloy.

The negative density of $-0.07 \mu_B/\text{atom}$ for or-

TABLE V. Summary of individual magnetic-moment results for NiFe and AuFe alloys.^a

Alloy	$\frac{\mu_B}{\text{Fe}}$	$\frac{\mu_B}{\text{Ni}}$	$\bar{\mu}_{3d}$	$\bar{\mu}_{\text{macro}}^b$	$\frac{\mu_B}{\text{Fe}}^c$	$\frac{\mu_B}{\text{Ni}}^c$
$\text{Ni}_3\text{Fe}(\text{ord.})$	3.10	0.68	1.29	1.22 (Ref. 8)	2.97	0.62
$\text{Ni}_{0.75}\text{Fe}_{0.25}$	3.13	0.63	1.25	1.15 (Ref. 8)	2.91	0.60
$\text{Ni}_{0.5}\text{Fe}_{0.5}$	2.54	0.78	1.66	1.56 (Refs. 18 and 19)	2.60	0.67
$\text{Au}_{0.75}\text{Fe}_{0.25}$	2.84		0.71	0.67 (Ref. 12)		

^aAll moment values refer to room temperature except those for the AuFe alloy which are at 100 °K.

^bMagnetization results (individually referenced).

^cDiffuse neutron-scattering results (Ref. 20).

dered Ni_3Fe is the same as that obtained from the Fourier inversion at the position $\frac{1}{2}00$ ($-0.0062 \mu_B/\text{Å}^3 = -0.070 \mu_B/\text{atom}$). However, the inversion provides additional detail. The density maps in Fig. 2 show extensive regions of negative density around the equivalent positions $\frac{1}{2}00$, $0\frac{1}{2}0$, $00\frac{1}{2}$ but only a small negative region along with some structure around $\frac{1}{2}\frac{1}{2}\frac{1}{2}$. Each of these positions has six nearest-neighbor atoms at a distance of $\frac{1}{2}a_0$. Around the $\frac{1}{2}00$ -type positions there are two Fe and four Ni atoms, each of which has a highly populated d orbital (E_g 's of Fe and B_{1g} 's of Ni) directed toward that position. The six Ni atoms surrounding $\frac{1}{2}\frac{1}{2}\frac{1}{2}$ have their underpopulated (relative to a spherical distribution) A_{1g} orbitals directed toward that position. One might argue that the negative density between atoms is proportional to the d -like density on the atoms and that the $\frac{1}{2}00$ -type positions should therefore have the larger negative density according to the moment environments

just described. It is, however, difficult to reconcile this conclusion with the results for pure Ni^3 which show a uniform moment density of $-0.0085 \mu_B/\text{\AA}^3$ between atoms and for which all four of the above-mentioned positions have essentially the same near-neighbor moment environment as the $\frac{1}{2}\frac{1}{2}\frac{1}{2}$ position in ordered Ni_3Fe .

In the last two columns are the individual moment values obtained by Shull and Wilkinson²⁰ from diffuse-neutron-scattering measurements on disordered NiFe alloys. These results are independent of form-factor assumptions since the measurements were made in the small- K region where the form factors are converging toward unity. The agreement between the two sets of moment values provides assurance that reasonable form

factors were used in the analysis of the present data. We note that the nonlocal-moment density should be added to the Shull-Wilkinson values and this would further improve the over-all agreement. Hasegawa and Kanamori⁷ have calculated the band structure of ferromagnetic disordered NiFe alloys by the coherent-potential approximation. They successfully reproduce the composition dependence of the individual Fe and Ni moments.

These calculations also show a rapid decrease in the density of states at the Fermi level of the minority-spin Ni d band with the addition of Fe. Since this region is predominantly of T_{2g} character in pure Ni, this indicates a rapid decrease in the fractional population of the T_{2g} subband as Fe

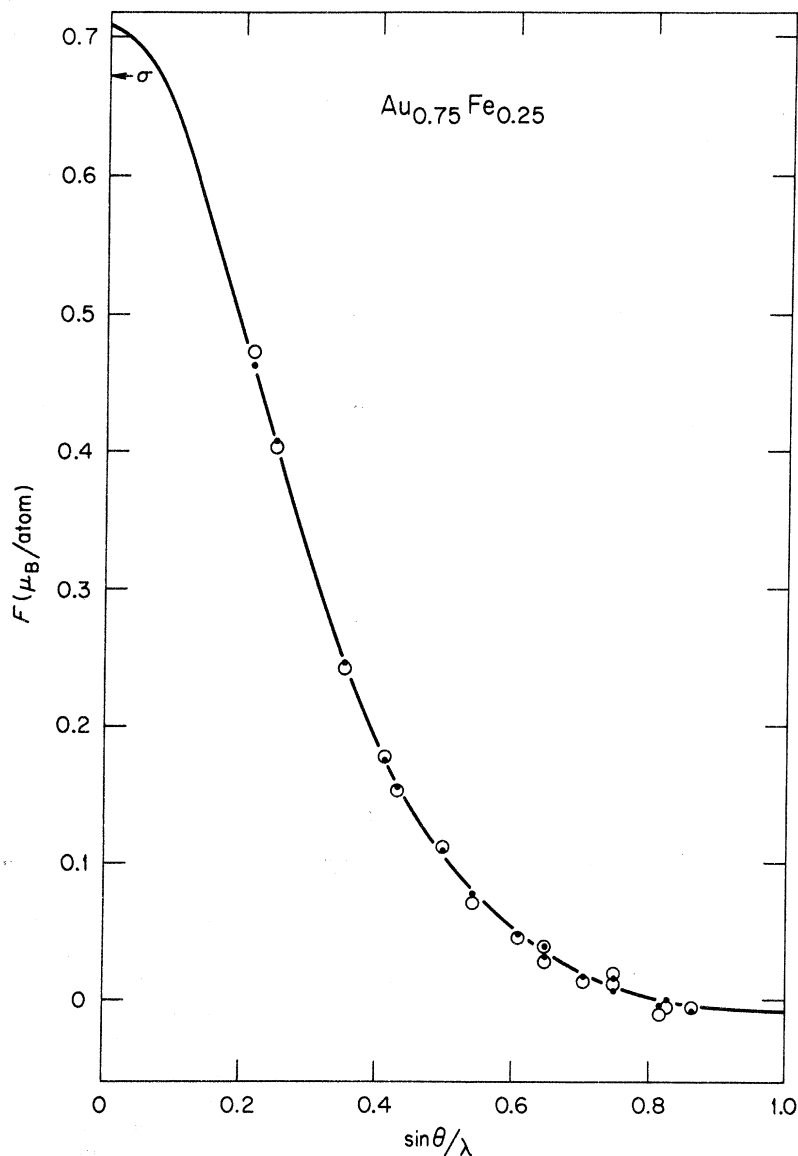


FIG. 6. Comparison of the observed (open points) and calculated (closed points) magnetic structure factors of disordered $\text{Au}_{0.75}\text{Fe}_{0.25}$.

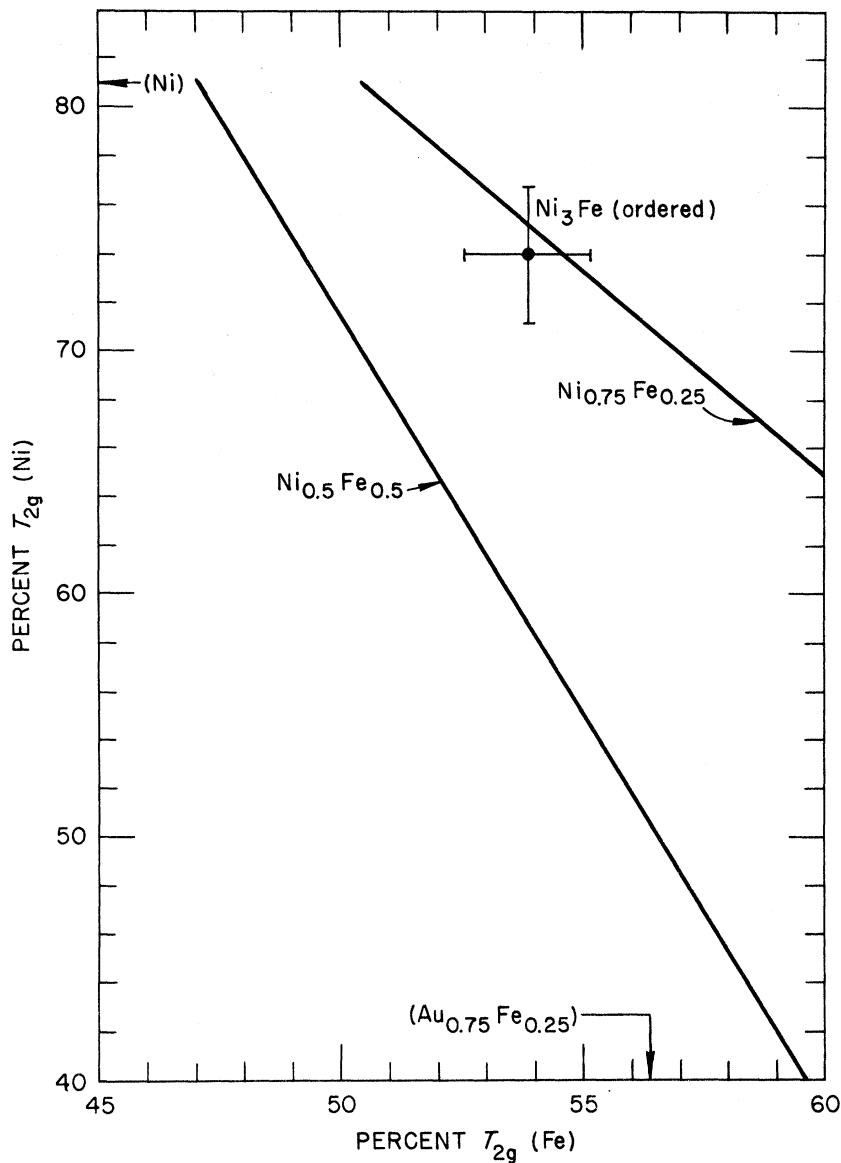


FIG. 7. T_{2g} character of the Fe and Ni atoms in NiFe and AuFe alloys.

is added to Ni. We now proceed to show that our symmetry results are consistent with this interpretation. These are presented in terms of the individual Fe and Ni T_{2g} character in Fig. 7. The individual determinations are shown by arrows for the 81% T_{2g} character of pure Ni and the 56% T_{2g} character of Fe in $\text{Au}_{0.75}\text{Fe}_{0.25}$ and also by the data point for ordered Ni_3Fe for which we take $T_{2g}(\text{Ni}) = B_{2g} + E_g$. As previously noted, only an average asymmetry parameter is determined for the disordered alloys. For these, the results are represented by lines of possible values consistent with the average T_{2g} character which has the form

$$\bar{T}_{2g} = [c_{\text{Fe}} \mu_{\text{Fe}} T_{2g}(\text{Fe}) + c_{\text{Ni}} \mu_{\text{Ni}} T_{2g}(\text{Ni})] / \bar{\mu}.$$

The most striking aspect of this plot is that the

data point for ordered Ni_3Fe falls on the line representing the possible T_{2g} populations for the disordered 25-at.% Fe in Ni alloy. This strongly suggests that the individual T_{2g} populations of 74% for Ni and 54% for Fe apply to both the ordered and disordered alloys. This is reasonable in view of recent band-structure calculations²¹ for ordered and disordered Cu_3Ni which show that the principal effect of disordering is to smooth out the sharp details of the density-of-states curve without changing the over-all features. This suggestion is further supported by the nearly identical $T_{2g}(\text{Fe})$ character of the AuFe alloy for which similar density-of-states arguments can be made. The $\text{Ni}_{0.5}\text{Fe}_{0.5}$ result is more ambiguous. Here the Fe moment is about 20% smaller than for the

other alloys and there is no assurance that the 54% $T_{2g}(\text{Fe})$ character should apply. However, given the decreasing trend in $T_{2g}(\text{Ni})$, this plot defines reasonable limits to the individual asymmetries for this alloy. These are 50–54% for $T_{2g}(\text{Fe})$ and 58–72% for $T_{2g}(\text{Ni})$. These symmetry results are qualitatively in accord with the calculations of Hasegawa and Kanamori. However, their calculations suggest a more rapid decrease of $T_{2g}(\text{Ni})$ than is observed.

The source of this changing T_{2g} character can be seen by comparison of the percentage populations of the Ni d functions in pure Ni³ with those in ordered Ni₃Fe. These are given in Table VI, from which it seems that the major effect of placing the Ni atom in the tetragonal environment of ordered Ni₃Fe is to shift some unpaired spin distribution from $d(xy)$ into $d(x^2 - y^2)$. We note that this occurs with little change in Ni moment. It is perhaps not surprising that the $d(xz)$ and $d(yz)$ functions are populated to the same extent since these are directed toward nearest-neighbor Ni atoms in both systems. The $d(xy)$ functions are also directed toward nearest neighbors but these are Fe atoms in Ni₃Fe. Apparently, the presence of these Fe atoms causes a reduction in the $d(xy)$ component of the Ni moment. We attribute this to the larger size of the Fe atom [see Figs. 1 and 2(b)] and to a repulsion of spin-up electrons away from the

TABLE VI. Percentage population of the Ni d orbitals in Ni and in ordered Ni₃Fe.

	Ni	Ni ₃ Fe
$d(x^2)$	$9\frac{1}{2}$	8 A_{1g}
$d(x^2 - y^2)$	$9\frac{1}{2}$ } E_g	18 B_{1g}
$d(xy)$	27	18 B_{2g}
$d(xz)$	27 } T_{2g}	28 } E_g
$d(yz)$	27	28

regions of stronger $d-d$ overlap. In the disordered alloys this repulsive effect would be distributed among the T_{2g} set of d functions. Extrapolation of the observed effect for the ordered alloy into the disordered regime by the assumption of a linear response to the number of nearest-neighbor Fe atoms would indicate 76 and 71% $T_{2g}(\text{Ni})$ populations for the alloys with 25 and 50% Fe, respectively. The corresponding $T_{2g}(\text{Fe})$ populations from Fig. 7 are 53 and 50%. This suggests that $T_{2g}(\text{Fe})$ also decreases as the number of Fe-Fe first-neighbor pairs increase.

ACKNOWLEDGMENTS

The authors are indebted to Dr. R. M. Moon for performing the Fourier sums and to Dr. H. R. Child for some of the least-squares-fitting calculations.

*Research sponsored by the U. S. Atomic Energy Commission under contract with the Union Carbide Corp.

†Consultant.

¹C. G. Shull and Y. Yamada, J. Phys. Soc. Japan **17**, Suppl. 1 (1962).

²R. M. Moon, Phys. Rev. **136**, A195 (1964).

³H. A. Mook, Phys. Rev. **148**, 495 (1966).

⁴B. Antonini, F. Menzinger, A. Paoletti, and F. Sacchetti, Intern. J. Magnetism **1**, 183 (1971).

⁵S. Wakoh and J. Yamashita, J. Phys. Soc. Japan **21**, 1712 (1966).

⁶L. Hodges, H. Ehrenreich, and N. D. Lang, Phys. Rev. **152**, 505 (1966).

⁷H. Hasegawa and J. Kanamori, J. Phys. Soc. Japan **31**, 382 (1971).

⁸R. J. Wakelin and E. L. Yates, Proc. Phys. Soc. (London) **B66**, 221 (1953).

⁹V. I. Gomankov, I. M. Puzey, and A. A. Loshmanov, Phys. Met. Metallogr. **22**, 134 (1966).

¹⁰R. G. Treuting and B. W. Batterman, J. Appl. Phys. **34**, 2005 (1963).

¹¹R. Nathans, C. G. Shull, G. Shirane, and A. Andreassen, J. Phys. Chem. Solids **10**, 138 (1959).

¹²J. Crangle and W. R. Scott, J. Appl. Phys. **36**, 921 (1965).

¹³R. M. Moon, Intern. J. Magnetism **1**, 219 (1971).

¹⁴R. J. Weiss and A. J. Freeman, J. Phys. Chem. Solids **10**, 147 (1959).

¹⁵R. E. Watson and A. J. Freeman, Acta Cryst. **14**, 27 (1961).

¹⁶A. J. Freeman (private communication).

¹⁷B. Antonini, F. Lucari, F. Menzinger, and A. Paoletti, Phys. Rev. **187**, 611 (1969).

¹⁸J. Crangle and G. C. Hallam, Proc. Roy. Soc. (London) **A272**, 119 (1963).

¹⁹J. W. Cable and E. O. Wollan, Intern. J. Magnetism **2**, 1 (1972).

²⁰C. G. Shull and M. K. Wilkinson, Phys. Rev. **97**, 304 (1955).

²¹J. Yamashita, S. Wakoh, and S. Asano, J. Phys. Soc. Japan **31**, 1620 (1971).